Distribution of Silicates and Ices in Callisto

J. D. Anderson*, G. Schubert†, R. A. Jacobson*, E. L. Lau*,

W. B. Moore† & W. L. Sjogren*

*Jet Propulsion Laboratory, California Institute of Technology, Pasadena, California 91109-8099, USA

†Department of Earth and Space Sciences, Institute of Geophysics and Planetary Physics, University of California Los Angeles, California 90095-1567, USA

20 February 1998

Abstract

Using radio Doppler data from a single encounter (C3) of the Galileo spacecraft with Callisto, we have reported previously that this outermost Galilean moon might be undifferentiated. Now, similar data from a second encounter (C9) corroborate this conclusion, but data from a third encounter (C10) suggest that there is some degree of differentiation in the compressed ice and rock (including iron and iron sulfide) that most likely make up the satellite. However, the degree of differentiation is nowhere near as extreme

as for Ganymede, where strong gravitational and magnetic evidence argues for separation of Ganymede into a metallic core, rock mantle, and ice–rich outer shell. On the basis of the C10 data, Callisto is most likely a partially differentiated ice–rock mixture with a rock fraction that increases modestly with depth. Also, the C10 data require that the ice and rock in Callisto not be completely separated, nor can Callisto be totally undifferentiated.

During the primary Galileo Orbiter mission, three close Callisto encounters provided data on the satellite's gravitational field [1]. Using radio Doppler data generated by the Deep Space Network (DSN) at three 70 meter stations located respectively at Goldstone California (DSS14), near Madrid Spain (DSS63), and near Canberra Australia (DSS43), and using nonlinear weighted least squares [2], we determined the second degree coefficients in the standard spherical harmonic expansion of the gravitational potential V [3]

In principle, the rotational and tidal distortions of Jupiter's Galilean satellites are separately excited and separately measurable. Hence it is possible to deduce the degree of central condensation in two independent ways [4]. For a satellite such as Callisto, in synchronous rotation with its orbital period, equilibrium theory predicts that the gravitational coefficient $J_2 \equiv -C_{20}$ is exactly 10/3 of C_{22}. Any significant deviation from this exact relationship indicates that the assumption of hydrostatic equilibrium is not appropriate. Unfortunately, the three Callisto flybys are so nearly equatorial that little or no information can be extracted for J_2. However, as we pointed out previously [5], it is unlikely that the rigidity of materials that make up Callisto could hide a strongly differentiated satellite, given that the C3 data infer an extreme upper limit for C_{22}.

Some pertinent data for the three Callisto encounters are given in Table 1. The location of

the spacecraft's closest approach is given in the first three rows, where longitude is measured west of the Callisto–Jupiter direction and altitude is referenced to a sphere of radius R = 2403 km [3]. The SEP angle is the elongation between the Sun and Jupiter. For SEP angles greater than 90 degrees, the minimum amount of phase noise is introduced into the S– band (2.3 GHz) radio wave as it propagates through solar plasma [6]. The next three rows give the direction cosines of the Doppler line of sight for the Callisto flyby trajectory at closest approach. The cross–track component is aligned with the Callisto–spacecraft direction, the along–track component is aligned with the spacecraft's Callisto–centered velocity vector, and the normal component is aligned with the spacecraft's Callisto–centered orbital angular momentum vector. The geometry is most favorable for C3, where both along–track and cross–track components of the Doppler shift can be detected. The line of sight for C9 is mostly cross–track because the spacecraft passed directly behind Callisto (Earth occultation), hence the favorable altitude for C9 is not accessible to the radio system. The altitude at occultation ingress is 1473 km and the altitude at egress is 1103 km. For C10 the spacecraft passed directly in front of Callisto, although radio Doppler data were obtained for the entire critical period around closest approach (Fig. 1). However, any gravitational perturbations for C9 and C10 are detected by the Callisto–centered trajectory bending only, while for C3 both the bending and the velocity perturbation along the orbital path contribute to the measured Doppler shift.

The next two rows of Table 1 give information on the quality of the available radio Doppler data. The most important criterion is whether or not the data are coherent with hydrogen maser frequency standards at the DSN complexes. This coherency is achieved only when the spacecraft radio system is locked to a signal from a DSN station by means of its

S-band transponder. Otherwise, the data are referenced to the spacecraft's crystal oscillator with its inherently poor frequency stability, unknown frequency bias, and unknown frequency drift, in comparison to atomic frequency standards. In fitting C3 and C9 data we include the bias and drift as parameters in the model. These two parameters are unnecessary for the coherent C10 data. Other factors, most importantly the continuity of the data and the location of data gaps with respect to the closest approach time, also affect the data quality. The row labeled data grade, on a scale of 1 (fair) to 4 (excellent), represents our overall assessment of data quality.

Finally, the last four rows of Table 1 give the results of the data analysis, with each flyby analyzed independently. The estimated errors, both in the table and in the text, are taken directly from the covariance matrix associated with the data analysis. They are based on an assumed standard error of 2 mm s^{-1} for noncoherent Doppler and 1 mm s^{-1} for coherent Doppler at a sample interval of 60 s. For data sampled at 10 s the error is increased by the square root of six. A weighting algorithm is applied that down weights the data for lower elevation angles at the DSN stations.

Our result for C3 has been published before [5], but the results for C9 and C10 are new. The results for J_2 and C_{22} depend on the assumption that all other harmonics in the potential function V are zero. The coefficient J_2 has been constrained a-priori to 10/3 of C_{22} in the least squares fitting procedure. The coefficient μ represents the correlation between J_2 and C_{22} from the post-fit covariance matrix. The last row of Table 1 represents an estimate of the axial moment of inertia normalized to MR^2 from Radau-Darwin equilibrium theory [4]. It is not an independent parameter of the model, but is calculated from the inferred value of C_{22}. For a sphere of constant density, C/MR^2 is 0.4, hence the results from C3 and C9

indicate that Callisto is very nearly of homogeneous composition. However the result from C10 is definitely not consistent with a body of uniform density, and indicates that Callisto is centrally condensed.

The results of Table 1 are just barely consistent at the one–sigma level, and a weighted mean of the three results just returns the C10 value for C_{22}. For C3 the data are of only fair quality, but the geometry is excellent, while for C10 the data are excellent but the geometry is only fair. However, because of the excellent data from C10, we have more confidence in the lower value of C_{22}. This confidence is reinforced by an independent fit to all the Doppler data from the three Callisto encounters, along with ground–based astrometric data on the positions of all four Galilean satellites and optical navigational data from NASA's Voyager missions to Jupiter. This combined solution includes adjustments to the satellite ephemerides, obtained by numerical integration of their equations of motion, as well as to all the important sources of gravitation. We concentrate on the Callisto results here.

Because the given orientation of the satellite's axes predates the Voyager mission, we include all five second degree gravitational coefficients. The two harmonics C_{21} and S_{21} of first order can be interpreted as corrections to the orientation of the polar axis. If the x axis is aligned on average in the Callisto–Jupiter direction, along the smallest principal moment of inertia A, the coefficient S_{22} should be zero. We obtain the following values in units of 10^{-6}.

$$J_2 = 31.1 \pm 4.5$$

$$C_{21} = 0.0 \pm 0.4$$

$$S_{21} = 0.0 \pm 0.8$$

$$C_{22} = 10.5 \pm 0.4$$

$$S_{22} = -0.7 \pm 0.3$$

$$\mu = 0.202 \qquad (1)$$

The orientation of Callisto's axes needs no correction, with the possible exception of the x axis. However, a slight shift of the x axis on the equator to bring the solution into agreement with a zero value of S_{22} has an insignificant effect on the value of C_{22}. The a–priori constraint that J_2 is exactly 10/3 of C_{22} is retained within its one–sigma error bound. There is a low positive correlation $\mu = 0.202$ between J_2 and C_{22} after the fit, but this does not imply they are independently determined. A large variation in J_2 outside its error limits, even setting it equal to zero and leaving it out of the fit, produces an insignificant change to C_{22} and has essentially no effect on the Doppler residuals after the fit. The data analysis yields C_{22} as the only spherical harmonic of geophysical significance. It is one percent larger in (1), where data from the three encounters have been combined, than the value given in Table 1 from C10 alone. However, because of the more complete nature of the combined solution, we adopt $C_{22} = 10.5 \pm 0.4$ from (1), and use this slightly larger value in all the geophysical interpretation to follow.

Our adopted solution for Callisto's gravitational field fits the C9 and C10 Doppler data to the noise level, and leaves a small systematic trend in the C3 data. This systematic trend, also apparent in our previous results [5], explains the difference between the C_{22} values from C3 and C10 in Table 1. We conclude that the systematic trend in the C3 data is caused by errors outside Callisto's gravitational field. The fact that the longitudes are about the same for C3 and C10 rules out gravity anomalies as a source. Possible sources of systematic

error in the C3 Doppler data include a random walk in the spacecraft oscillator's frequency, variations in solar plasma at the smaller SEP angle on a time scale of 15 minutes, or high-frequency errors in Jupiter's ephemeris on the same time scale. The C9 data include an Earth occultation, with a corresponding gap in the Doppler data at closest approach, so it is relatively easier to fit the C9 data with the C10 value of C_{22}.

We use the measured value of C_{22} and the average density to infer the internal structure of Callisto on the assumption that the moon's spherical harmonic degree 2 gravitational field is due to the equilibrium tidal and rotational ellipsoidal distortion of a satellite in synchronous rotation with its orbital period. Under these conditions, C_{22} is related to the rotational parameter q_r by

$$C_{22} = \frac{3\alpha q_r}{4} \tag{2}$$

where q_r is a measure of the forcing for rotational flattening of the satellite ($q_r = 36.69 \times 10^{-6}$ for Callisto) and α is a dimensionless response coefficient that depends on the distribution of density with depth inside the satellite ($\alpha = 0.5$ for constant density) [4]. For $C_{22} = 10.5 \pm 0.4$ in units of 10^{-6}, α is 0.382 ± 0.015. From equilibrium theory and the value of α, it follows that Callisto's axial moment of inertia C, normalized to MR^2, is $C/MR^2 = 0.359 \pm 0.005$. This value of C/MR^2 is substantially less than 0.4, the value of C/MR^2 for a sphere of constant density, and requires some concentration of mass toward the center of Callisto. The value of C/MR^2 we reported after the C3 flyby [5] was consistent with an object of constant density and we inferred from the C3 data alone that Callisto was not differentiated [5]. The present data, however, require some differentiation of the satellite as we discuss more quantitatively below. It can be immediately appreciated though, by comparing Callisto with Ganymede,

that the degree of differentiation in Callisto is not large. Ganymede and Callisto are both icy satellites (mixtures of roughly equal amounts of ice and rock/metal, [7]) with comparable radii and densities. The C/MR^2 of Ganymede is 0.3105 ± 0.0028 [8], much smaller than the value of C/MR^2 for Callisto. Ganymede's mean density and low value of C/MR^2 together with its intrinsic magnetic field [9] imply that it is fully differentiated into a metallic core surrounded by a rock mantle and an outer ice shell [8, 10]. In contrast, Callisto's ice and rock cannot be fully separated since that would require Callisto to have a C/MR^2 value as small as that of Ganymede. Callisto's ice and rock are only partially separated. As quantified below, Callisto is a partially differentiated ice–rock body with a rock fraction that increases with depth.

That Callisto must be partially differentiated can be readily appreciated by calculating the C/MR^2 of an undifferentiated model of Callisto with constant ice-rock fraction. Since the ice in such a model of Callisto would undergo transformation with depth to higher density phases [7], the density of an undifferentiated model of Callisto would actually increase with depth and the C/MR^2 of the model would be less than 0.4. The amount of the decrease below 0.4 is small, however, and we ignored it in our previous discussion [5] of the C3 data because of the relatively large uncertainty in the C3 value of C_{22}. However, here the magnitude of the decrease is important because of the small uncertainties in C_{22} and the inferred value of C/MR^2. Undifferentiated models of Callisto involve transformations of ice to phases such as ice II, ice VI, and ice VIII at depth in the satellite [7, 11]. Other phases of ice (ice III and ice V) may occur depending on the radial profiles of temperature and pressure in the model interiors. The depths of the ice phase changes also depend on the temperature and pressure profiles. Accordingly, the C/MR^2 values of undifferentiated Callisto models vary

with model details, but typical values are in the range 0.385 – 0.39. McKinnon [12] calculates an undifferentiated model of Callisto with $C/MR^2 = 0.38$. Even the 0.38 value of C/MR^2 is more than 4 σ away from the nominal value of $C/MR^2 = 0.359$ reported here, leaving little doubt that Callisto must be partially differentiated.

Consistent with the few constraints we have on Callisto's internal structure (mean density and moment of inertia), we explore simple 2–layer and 3–layer models of its interior density. We solve Clairaut's equation for the distortion of the model to the tidal and rotational potentials and determine the family of model parameters consistent with the observed value of α. There are more model parameters than available constraints, even for a 2–layer model, and no unique model of Callisto's internal mass distribution can be determined. Instead, we restrict the model parameter space with reasonable assumptions about the nature of Callisto's interior.

Possible 2-layer models of Callisto are shown in Fig. 2. The curves labelled with the values of C_{22} define the 2–layer models having the indicated values of C_{22}. The solid curve is the nominal value of C_{22} and the dashed curves represent the $\pm 1\sigma$ values of C_{22}. The lines labelled 100, 200, etc., give the outer shell thickness in kilometers. The range of outer shell densities on the vertical axis encompasses the densities of pure ice I, more compressed phases of ice, and ice-rock mixtures. The range of interior densities on the horizontal axis includes the densities of ice–rock mixtures and rock–metal. The average density of Callisto is 1830 kg m^{-3}. We restrict our discussion to models of Callisto confined between the $\pm 1\sigma$ values of C_{22}. For the smaller values of outer shell density, corresponding to a relatively rock–depleted ice outer shell, the outer shell thickness varies from about 200 km to about 400 km and the inner layer density is between about 2200 kg m^{-3} and 2400 kg m^{-3}. The

permissible interior densities are well below the densities of silicates and not much larger than the average density of Callisto, indicative of only a modest increase in rock fraction with depth. As outer shell density increases, outer shell thickness and interior density of possible Callisto models also increase, reaching values as large as about 900 km and about 3000 kg m^{-3}, respectively, for an outer shell density of 1500 kg m^{-3} (for the nominal value of C_{22} these values are about 800 km and 2750 kg m^{-3}). Models of Callisto having interior rock–like densities are therefore possible, but such models must also have thick (about 0.5 $R_{Callisto}$) outer shells that are ice–rock mixtures with substantial rock fractions. This class of models is discussed further when we consider 3–layer Callisto structures but we note here, from an evolutionary point of view, that these models are less plausible than partially differentiated models with ice-rock centers.

The degree of ice–rock differentiation in Callisto has also been assessed using a model in which the interior is an ice–rock mixture with a rock fraction that decreases exponentially with radial distance from the center of the model. Both the ice and rock are compressible and the ice is allowed to undergo solid state phase changes according to the phase diagram of Hobbs [13]. The model is isothermal and the depth dependence of the pressure is determined from the hydrostatic equation. Since the top down freezing of an outer ice Ih layer excludes impurities, this ice phase has been assumed devoid of rock. The maximum rock fraction at the center of the model, the uncompressed density of the rock, and the scale–height of the decrease of rock fraction with radius are parameters of the model. Fig. 3 delineates the models of this class that satisfy the mean density and C_{22} constraints. Central rock fraction and uncompressed rock density of possible Callisto models are indicated on the axes of the diagram, while the curves labelled 3000, 4000, etc. give the rock fraction scale height in

kilometers. Any point on the solid curve labelled 10.5 is a possible Callisto model having the nominal value of C_{22}. The dashed curve labelled 10.1 is the locus of possible Callisto models having the 1 σ lower estimate of C_{22}. For the nominal value of C_{22} and uncompressed rock density 3000 kg m^{-3} or larger, there must be ice at the center of the Callisto model since the maximum rock fraction is smaller than 0.85. Also, the rock fraction decreases relatively little with radius in these models since the scale height for the decrease is larger than about 5000 km compared with Callisto's radius of 2403 km [3]. Central rock fraction decreases and rock fraction scale height increases with increasing uncompressed rock density in these models. The 1 σ lower bound on C_{22} allows there to be Callisto models with no ice at the center for uncompressed rock density less than about 3300 kg m^{-3}. In general, the models with rock fraction exponentially dependent on radius lead to similar conclusions as do the 2-layer models. Though ice and rock cannot be completely separated in Callisto, the satellite must nevertheless be partially differentiated with the most plausible interior model involving a modest increase of rock fraction with depth.

The 3-layer models shown in Fig. 4 facilitate a more detailed investigation of the conditions under which Callisto could have a dense core. For illustrative purposes we assume that the models have a core with the density of Fe-FeS (5500 kg m^{-3}). Any point on the surface in Fig. 4 is a possible model of Callisto. The coordinate axes give other characteristics of the model, ice density or density of the outer layer, fractional core radius, and rock density or density of the middle layer. The color of the surface gives the thickness of the ice or outer layer. If the outer layer of the model is relatively ice-rich (small values of ice density) the layer can only be several hundred kilometers thick and the middle or rock layer must have density less than about 2300 kg m^{-3}. In other words, the middle layer must be an ice-rock

mixture with comparable amounts of both ice and rock. The radius of the core must be less than about 0.4 $R_{Callisto}$ and the density of the middle layer must decrease, or its ice fraction must increase, as the core radius increases. Since the core in these models is limited in radius to 0.4 $R_{Callisto}$ and the outer layer is only a few hundred kilometers thick, the middle ice-rock layer must be about 0.5 $R_{Callisto}$ thick. All the models with cores and ice–rich outer layers have thick middle layers of ice–rock mixtures with about equal amounts of ice and rock. The yellow–orange part of the surface shows that there are models with middle layers having large densities typical of rock/metal. But these models have outer layers that are about 0.5 $R_{Callisto}$ thick and composed of an ice–rock mixture with comparable amounts of ice and rock. These models are equivalent to the ones at the opposite end of the surface in Fig. 4 in that both have dense deep interiors surrounded by thick exteriors of ice and rock.

The viability of the dense deep interior models of Callisto must be determined by evolutionary considerations. If Callisto accreted homogeneously as an ice–rock mixture and subsequently differentiated as a result of accretional heating or radiogenic heating in the rock component, then we consider it unlikely that Callisto could have differentiated a dense rock/metal core while maintaining its outer half by radius as a primordial ice–rock mixture, as required by its mean density and moment of inertia. Instead, it seems more plausible that Callisto partially differentiated its ice–rock mixture through accretional or radiogenic heating with some of the rock from the outer parts of the satellite separating, sinking, and accumulating at depth.

A model of Callisto in which there has only been partial ice–rock differentiation with rock fraction increasing relatively modestly with depth is consistent with other observations of the satellite. Callisto does not have an intrinsic magnetic field [14], which is consistent

with the absence of a metallic core. Callisto's surface shows no sign of endogenic activity consistent with a quiescent undifferentiated or partially differentiated interior [7]. Recent high resolution Galileo images of Callisto reveal no volcanic or tectonic features that could be associated with internal activity (J. Klemaszewski, private communication). In contrast, Ganymede, whose gravitational and magnetic fields suggest complete differentiation of the satellite into a metallic core, rock mantle and ice crust [10], has a surface that has been heavily modified by endogenic tectonism [7, 15]. High resolution Galileo coverage of Callisto is incomplete, and some areas identified in Voyager data as possibly modified by volcanic or internal tectonic activity [16], may yet turn out to be areas of degraded ancient tectonism associated with the early partial differentiation of Callisto (J. Klemaszewski, private communication). It is unlikely, however, that Callisto could have undergone substantial internal differentiation while leaving little or no evidence of this on its surface. Callisto is dynamically isolated from the three inner Galilean satellites and therefore lacks the tidal heat source that has driven the intense volcanic activity [7, 17] and large degree of differentiation [18] of Io and that may have played a role in the differentiation of Europa and Ganymede [7, 10, 19]. The possibility that tidal heating could have influenced the evolution of Ganymede but not of the similarly large and massive Callisto is perhaps the best way to reconcile the total differentiation of Ganymede with the partial differentiation of Callisto [5].

Acknowledgments.

This work was sponsored by the Galileo Project and was performed at the Jet Propulsion Laboratory, California Institute of Technology, under contract with the National Aeronautics

and Space Administration. G.S. and W.B.M. acknowledge support by grants from NASA through the Galileo Project at JPL and the Planetary Geology and Geophysics program.

References

[1] The first encounter (C3) occurred on 4 November 1996 at 11:47:09, the second (C9) occurred on 25 June 1997 at 13:47:50, and the third (C10) occurred on 17 September 1997 at 00:18:55, where the encounter times are expressed in Universal Time Coordinated (UTC) at the spacecraft, and the encounter designation Cn refers to an encounter with Callisto on the spacecraft's nth orbital revolution.

[2] See, for example, T. D. Moyer, *Tech. Rep. No. TR 32-1527* (Jet Propulsion Laboratory, Pasadena, CA, 1971); B. D. Tapley, in *Recent Advances in Dynamical Astronomy*, B. D. Tapley and V. Szebehely, Eds. (Reidel, Dordrecht, Netherlands, and Boston, MA, 1973), pp. 396–425; J. D¿ Anderson, in *Experimental Gravitation*, B. Bertotti, Ed. (Academic Press, New York, 1974), pp. 163–199.

[3] W. M. Kaula, *Theory of Satellite Geodesy* (Blaisdell, Waltham, MA, 1966). The expression for V is

$$V(r,\phi,\lambda) = \frac{GM}{r}\left[1 + \sum_{n=2}^{\infty}\sum_{m=0}^{n}\left(\frac{R}{r}\right)^n (C_{nm}\cos m\lambda + S_{nm}\sin m\lambda)\, P_{nm}(\sin\phi)\right] \qquad (3)$$

where M is the satellite's mass and G is the gravitational constant, G = 6.6728 ± 0.0016 × 10^{-11} m^3 kg^{-1} s^{-2}, E. R. Cohen, B. N. Taylor, *Phys. Today* **49**, BG9 (1996). The spherical coordinates (r, ϕ, λ) are referred to the center of mass, with r the radial distance, ϕ the latitude and λ the longitude on the equator. Callisto's reference radius

R is 2,403 km, M. E. Davies, V. K. Abalakin, A. Brahic, M. Bursa, B. H. Chovitz, J. H. Lieske, P. K. Seidelmann, A. T. Sinclair, Y. S. Tjuflin, *Celes. Mech.* **53**, 377 (1992). P_{nm} is the associated Legendre polynomial of degree n and order m, and C_{nm} and S_{nm} are the corresponding coefficients determined from the data.

[4] W. B. Hubbard, J. D. Anderson, *Icarus* **33**, 336 (1978); S. F. Dermott, *Icarus* **37**, 310 (1979); V. N. Zharkov, V. V. Leontjev, A. V. Kozenko, *Icarus* **61**, 92 (1985); S. Mueller, W. B. McKinnon, *Icarus* **76**, 437 (1988); G. Schubert, D. Limonadi, J. D. Anderson, J. K. Campbell, G. Giampieri, *Icarus* **111**, 433 (1994).

[5] J. D. Anderson, E. L. Lau, W. L. Sjogren, G. Schubert, W. B. Moore, *Nature* **387**, 264 (1997).

[6] R. Woo, J. W. Armstrong, *J. Geophys. Res.* **84**, 7288 (1979).

[7] G. Schubert, D. J. Stevenson, K. Ellsworth, *Icarus* **47**, 46 (1981); G. Schubert, T. Spohn, R. T. Reynolds, in *Satellites*, J. A. Burns, M. S. Matthews, Eds. (Univ. Arizona Press, Tucson, 1986) pp. 629–688.

[8] J. D. Anderson, E. L. Lau, W. L. Sjogren, G. Schubert, W. B. Moore, *Nature* **384**, 541 (1996).

[9] M. G. Kivelson, K. K. Khurana, C. T. Russell, R. J. Walker, J. Warnecke, F. V. Coroniti, C. Polanskey, D. J. Southwood, G. Schubert, *Nature* **384**, 537 (1996).

[10] G. Schubert, K. Zhang, M. G. Kivelson, J. D. Anderson, *Nature* **384**, 544 (1996).

[11] M. J. Lupo, *Icarus* **52**, 40 (1982); J. Leliwa-Kopystynski, L. Makkonen, O. Erikoinen, K. J. Kossacki, *Planet. Space Sci.* **42**, 545 (1994).

[12] W. B. McKinnon, *Icarus* **130**, in press (1998).

[13] P. V. Hobbs, *Ice Physics* (Clarendon Press, Oxford, 1974).

[14] K. K. Khurana, M. G. Kivelson, C. T. Russell, R. J. Walker, D. J. Southwood, *Nature* **387**, 262 (1997).

[15] S. W. Squyres, S. K. Croft, in *Satellites*, J. A. Burns, M. S. Matthews, Eds. (Univ. Arizona Press, Tucson, 1986) pp. 293–341; W. B. McKinnon, E. M. Parmentier, *ibidem* pp. 718–763; R. T. Pappalardo, J. W. Head, G. C. Collins, R. L. Kirk, G. Neukum, J. Oberst, B. Giese, R. Greeley, C. R. Chapman, P. Helfenstein, J. M. Moore, A. McEwen, B. R. Tufts, D. A. Senske, H. H. Breneman, K. Klaasen, *Icarus*, submitted (1998); G. C. Collins, J. W. Head, R. T. Pappalardo, *Geophys. Res. Lett.* **25**, 233 (1998); L. M. Prockter, J. W. Head, D. A. Senske, R. T. Pappalardo, G. Neukum, R. Wagner, U. Wolf, J. Oberst, B. Giese, J. M. Moore, C. R. Chapman, P. Helfenstein, R. Greeley, H. H. Breneman, M. J. S. Belton, *Icarus*, submitted (1998).

[16] P. M. Schenk, *Jour. Geophys. Res.* **100**, 19023 (1995).

[17] S. J. Peale, P. Cassen, R. T. Reynolds, *Science* **203**, 892 (1979); M. Segatz, T. Spohn, M. N. Ross, G. Schubert, *Icarus* **75**, 187 (1988); M. N. Ross, G. Schubert, *Icarus* **64**, 391 (1985).

[18] L. Keszthelyi, A. McEwen, *Icarus*, in press (1998); A. S. McEwen, L. Keszthelyi, P. Geissler, D. P. Simonelli, M. H. Carr, T. V. Johnson, K. P. Klassen, H. H. Breneman,

T. J. Jones, J. M. Kaufman, K. P. Magee, D. A. Senske, M. J. S. Belton, G. Schubert, *Icarus*, submitted (1998).

[19] R. Malhotra, *Icarus* **94**, 399 (1991); A. P. Showman, R. Malhotra, *Icarus* **127**, 93 (1997); A. P. Showman, D. J. Stevenson, R. Malhotra, *Icarus* **129**, 367 (1997).

Figure Captions

Fig. 1. Doppler residuals (observed Doppler velocity minus model Doppler velocity) at C10 for a model in which Callisto's gravitational field is represented only by GM and J_2. All other gravitational harmonics are zero. There is a strong residual signature which indicates that the model is incomplete. Although not shown, by adding one gravitational harmonic, C_{22}, the residuals are distributed randomly about zero Doppler velocity. Hence by including GM, J_2, and C_{22} in the model, the Doppler data can be fit to the noise level (0.3 mm s^{-1}, one σ, at a sample interval of 10 s). The best–fit value for C_{22} is $(10.5 \pm 0.4) \times 10^{-6}$ as explained in the text. The lower noise in the residuals near the beginning and end of the plot is caused by a larger sample interval of 60 s, and hence a longer Doppler integration time, compared to the sample interval of 10 s for the data surrounding the spacecraft's closest approach to Callisto (indicated by the single large tick mark).

Fig. 2. Possible two–layer models of Callisto defined by values of the densities of the interior and outer shell. All models satisfy the mean density constraint. Models that lie along the curve labelled 10.5 (in units 10^{-6}) also satisfy the nominal C_{22} constraint. The dashed curves labelled 10.9 and 10.1 delineate models that satisfy the $\pm 1\sigma$ C_{22} constraint.The thin solid lines sloping downward to the right give outer shell thickness in km.

Fig. 3. Possible internal structures of Callisto defined by central rock fraction and uncompressed rock density for models in which the interior is an ice–rock mixture with a rock fraction that decreases exponentially with radial distance from the center. All

models satisfy the mean density constraint. Models that lie along the curve labelled 10.5 (in units of 10^{-6}) also satisfy the nominal C_{22} constraint.The dashed curve labelled 10.1 delineates models that satisfy the -1σ C_{22} constraint. The other curves give the scale height in km associated with the exponential dependence of rock fraction on radial position.

Fig. 4 Three–layer models of Callisto's interior. All models incorporate an Fe–FeS core of density 5500 kg m^{-3} and satisfy the average density and nominal C_{22} (10.5×10^{-6}) constraints. Possible models lie on the surface whose colors indicate the thickness of the outer ice–rock shell. Other model parameters are defined by the coordinate axes. The intersection of the surface with the core radius/ Callisto radius equal to zero plane is identical to the solid curve in Fig. 2.

Tables

TABLE 1. Callisto Encounter Geometry and Gravity Results

	C3	C9	C10
Latitude (deg)	13.2	-2.3	4.6
Longitude (deg)	77.9	259.2	78.7
Altitude (km)	1136	418	535
SEP (deg)	61.1	132.3	138.8
Direction Cosines for Line of Sight			
Cross Track	-0.655	0.994	-0.996
Along Track	0.734	-0.104	0.051
Normal	0.178	-0.037	0.078
Coherent Doppler?	No	No	Yes
Data grade (1–4)	1.5	1.0	4.0
J_2 (10^{-6})	47.7 ± 11.5	49.3 ± 13.0	33.9 ± 4.7
C_{22} (10^{-6})	14.3 ± 3.2	14.8 ± 3.7	10.4 ± 0.3
μ	0.9128	0.9327	0.1372
C/MR^2	0.407 ± 0.039	0.412 ± 0.044	0.358 ± 0.004

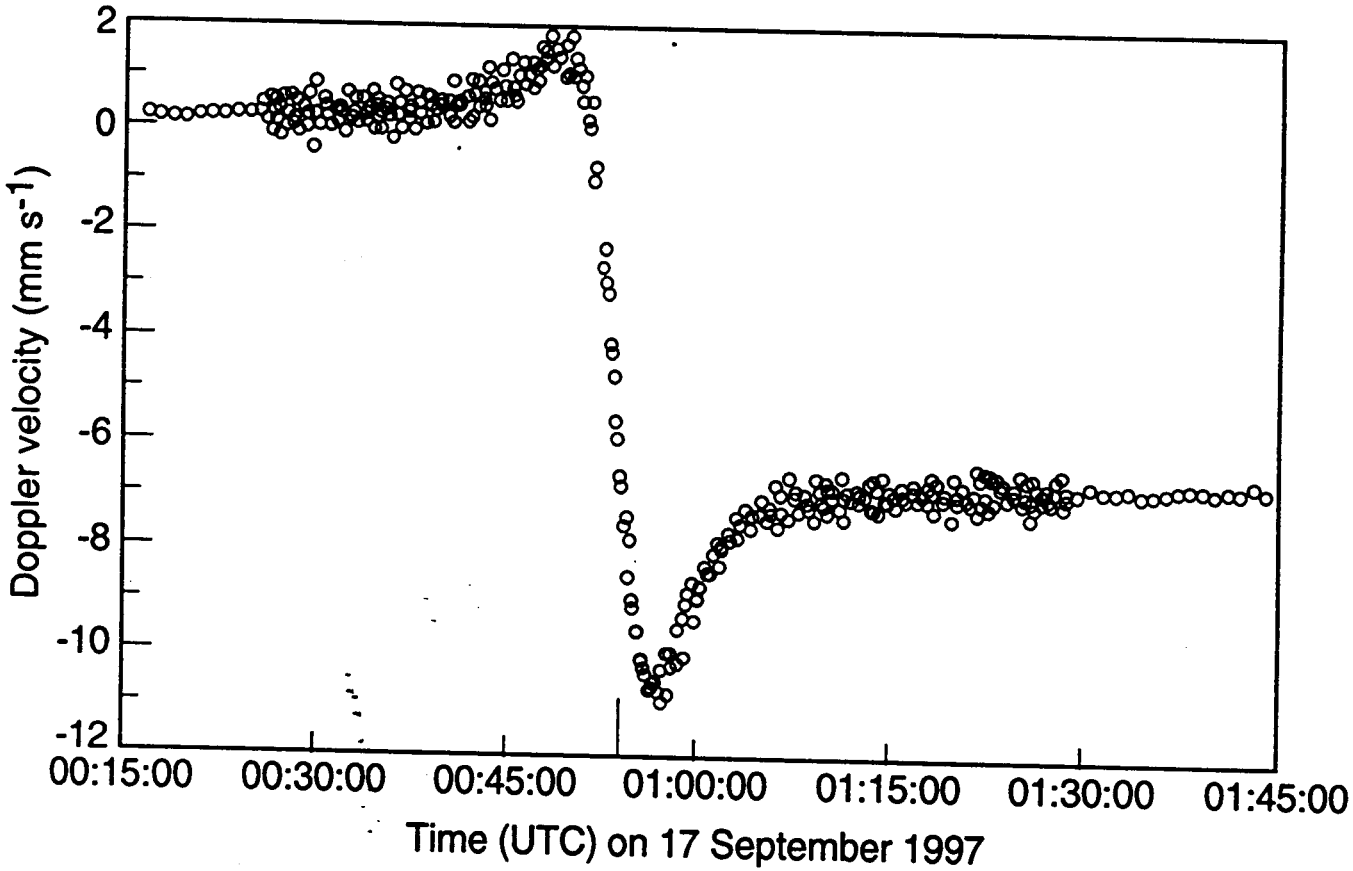
2
0
-2
-4
-6
-8
-10
-12
Doppler velocity (mm s-1)
00:15:00
00:30:00
00:45:00
01:00:00
01:15:00
01:30:00
01:45:00
Time (UTC) on 17 September 1997

Fig. 1

Fig. 2

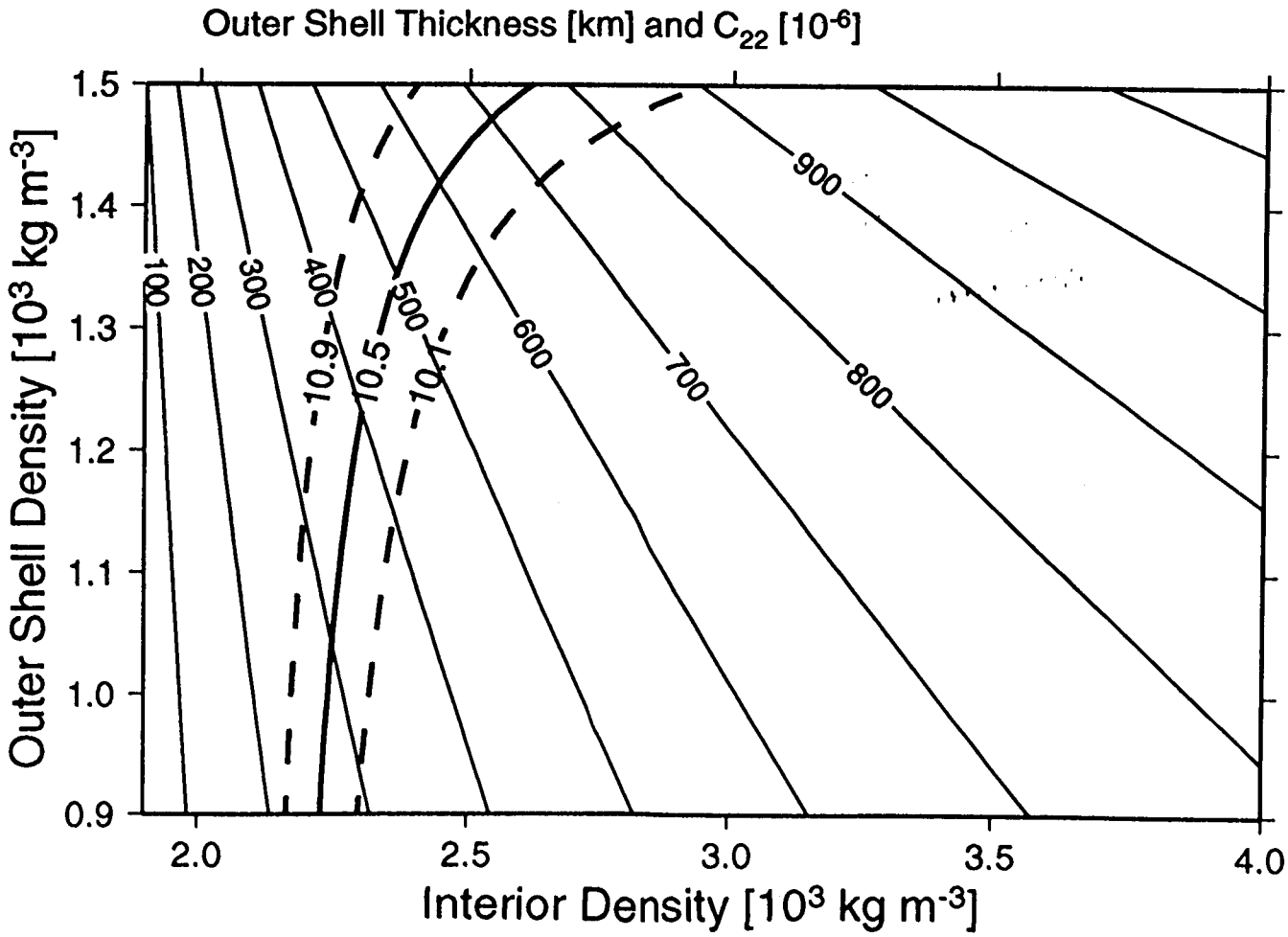
Outer Shell Thickness [km] and C_{22} [10^{-6}]
Outer Shell Density [10^3 kg m^{-3}]
Interior Density [10^3 kg m^{-3}]
1.5
1.4
1.3
1.2
1.1
1.0
0.9
2.0
2.5
3.0
3.5
4.0
100
200
300
400
500
600
700
800
900
-10.9
-10.5
-10.1

Fig. 3

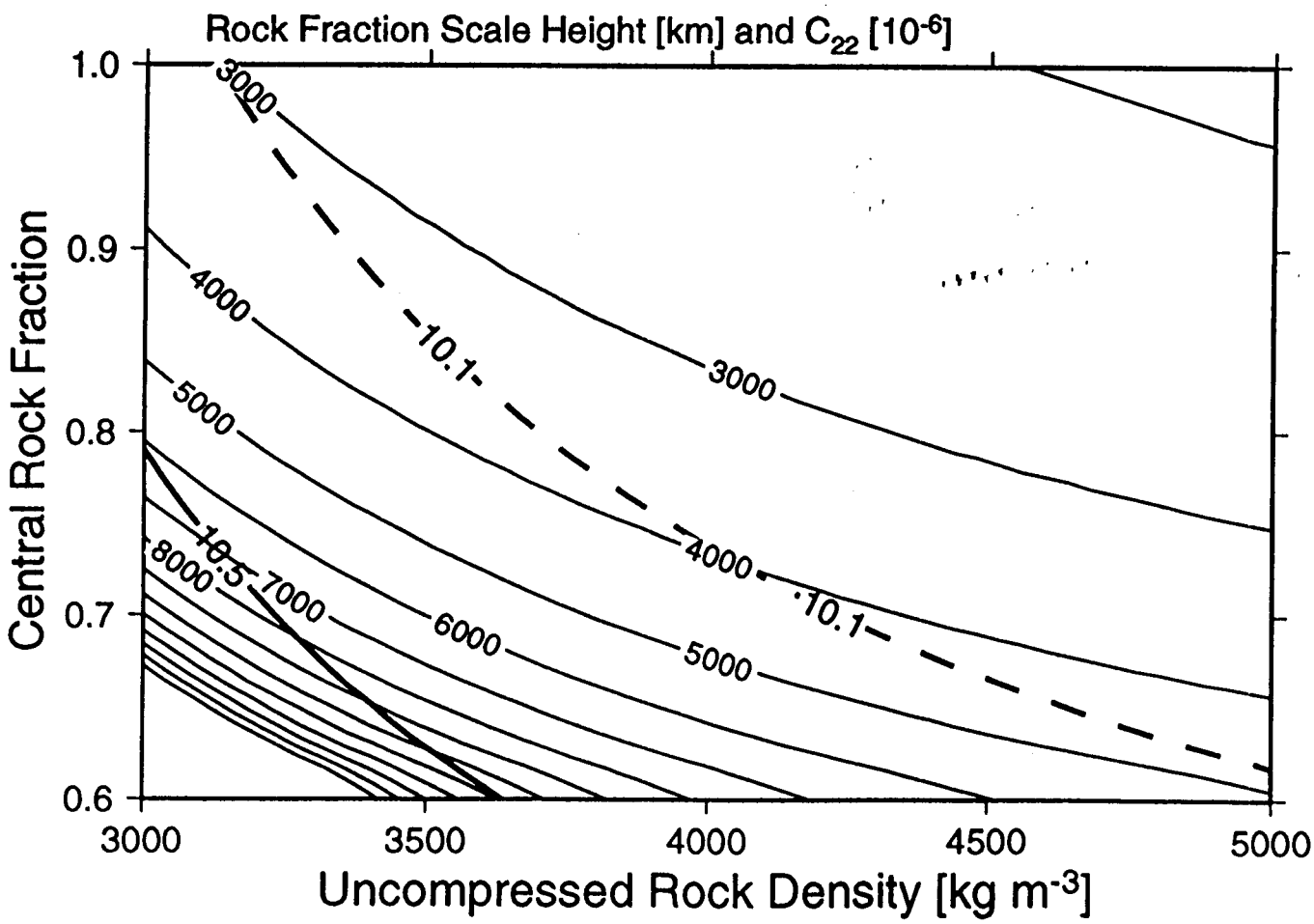
Rock Fraction Scale Height [km] and C_{22} [10^{-6}]
Central Rock Fraction
1.0
0.9
0.8
0.7
0.6
3000
3500
4000
4500
5000
Uncompressed Rock Density [kg m^{-3}]
3000
4000
5000
6000
7000
8000
10.1
10.1
10.5

Fig. 4

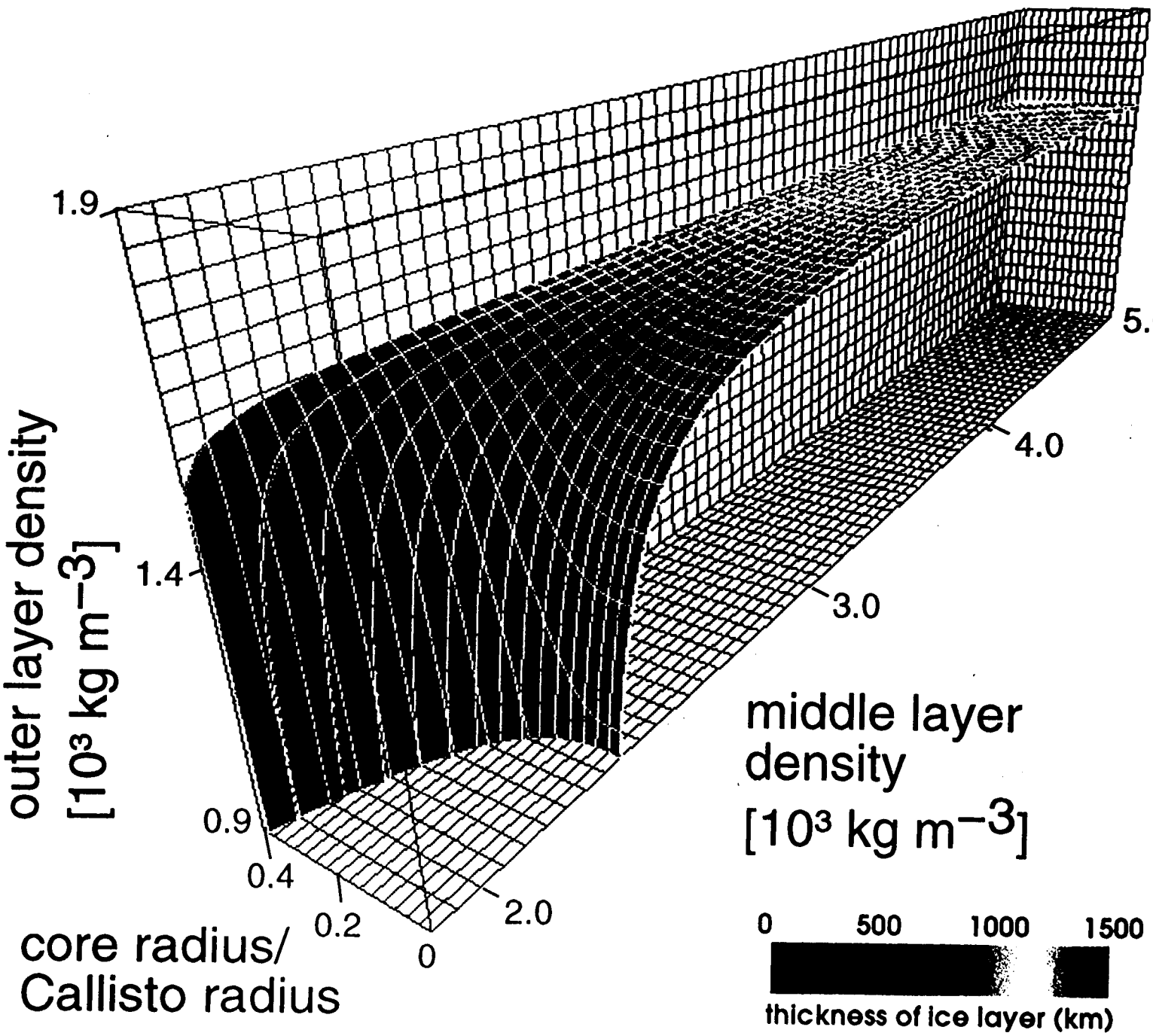
1.9
1.4
0.9
0.4
0.2
0
2.0
3.0
4.0
5.(
outer layer density
[10³ kg m⁻³]
middle layer
density
[10³ kg m⁻³]
core radius/
Callisto radius
0
500
1000
1500
thickness of ice layer (km)